Instrument: **SP1 Cooperation**

Thematic Priority: **Priority Area 1.1.6.3 "Global Change and Ecosystems"**

FP7 Collaborative Project – Grant Agreement 212492

CLARIS LPB
A Europe-South America Network for Climate Change Assessment and Impact Studies in La Plata Basin

DELIVERABLES

D6.2: Report on the results of the second annual workshop on extreme events including tables with frequency and intensity of extreme temperature and precipitation cases of 20th century (regional and global models and observation).

Due date of deliverable: Month 24

Start date of project: **01/10/2008** Duration: 4 **years**

Organization name of lead contractor for this deliverable: CONICET

Deliverable No	Deliverable title	WP	Lead beneficiary	Estimated indicative person-months (permanent staff)	Nature	Dissemination level	Delivery date
D6.2	Report on the results of the second annual workshop on extreme events including tables with frequency and intensity of extreme temperature and precipitation cases of 20th century (regional and global models and observation).	WP 6	P13-CONICET	23,20	R	PU	24

1. Introduction

The second WP6 workshop was help at Florianopolis (Brazil), from 8 to 9 November 2010. Seven researchers and students of WP6 participated presenting preliminary results of their works and discussing the ongoing activities on the main tasks of the extremes subproject: (T6.1) An investigation of the atmospheric features (large scale, synoptic and meso-scale systems), land surface-atmosphere, and ocean-atmosphere feedbacks, associated with the occurrence of extremes in precipitation and temperature; (T6.2) A quantification of observed and simulated trends in extremes; (T6.3) An assessment of the global warming influence on the statistics of the extremes. There were also cross-work-packages discussions including WP3, WP4 and WP5 with the aim of coordinate activities and plan for cross work-packages initiatives.

2. Participants

For WP6: Annalisa Cherchi (CMCC), Olga Penalba (UBA), Andrea F. Carril (CONICET), Grigory Nikulin (SMHI), Renata Tedeschi (UFP), da Rocha (USP), Armelle Remedio (MPI). For cross-work-package discussions participated Phil Jones, Andres Farrall and Jean-Phillipe Boulanger for WP3, Carolina Vera, Marcelo Barreiro and Renata Tedeschi for WP4 and Silvina Solman, Enrique Sanchez and Hugo Berberi for WP5.

3. Results of WP6 subproject

A summary of the presentations is displayed bellow.

3.1. UFP (Alice M. Grimm, Renata G. Tedeschi, Rafaela A. Flach and Aline B. G. Ingberman) in collaboration with CPTEC/INPE (Cavalcanti). Exploring the impact of Canonical and Modoki ENSO on extreme precipitation

ENSO episodes usually display characteristic patterns of SST anomalies, with warmer (colder) SST in the central-east equatorial Pacific for El Niño (La Niña) episodes. However, there are differences in these patterns from one to another episode. The main difference is related to the longitudinal position of the strongest SST anomalies: in most episodes they are in the eastern Pacific, but in some of them they are in the central Pacific. Ashok et al. (2007) studied a special type they called Modoki Niño, with strongest anomalies in the central Pacific.

We determined the difference between the impact on the frequency of extreme precipitation events caused by the canonical and Modoki ENSO over the LPB. Only parts of the results are shown here. The study was conducted on seasonal time scale, and the ENSO episodes were determined with the following criteria (Figure 1):

Modoki ENSO: This method is based on Ashok et al. (2007)

- Calculate EN Modoki index (EMI): EMI=$[SSTA]_A$-0.5$[SSTA]_B$-0.5$[SSTA]_C$ and chose the years in which EMI is greater (lesser) than 0,7σ_M and the anomaly in region A is greater (lesser) than 0,7σ_A : these are the EN (LN) Modoki years.

Canonical ENSO:

- If the anomaly of the canonic region is greater (lesser) than $0{,}7\sigma_{Can}$.

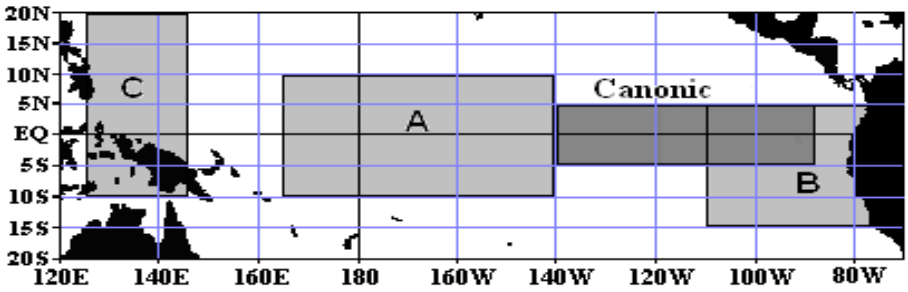

Figure 1. ENSO regions.

Figure 2 shows that during SON and MAM, when there is significant ENSO impact over the LPB, Canonical ENSO (ENC and LNC) and Modoki ENSO (ENM and LNM) have different impacts. SON: decrease of extreme events in the north of LPB and increase in the south during ENM. During LNM there are anomalies of opposite sign to ENM in the south and in the middle of LPB, but this composite is based on only two years. Canonical ENSO does not produce opposite anomalies in the northern and southern parts of the basin. MAM: weak increase of extreme events in the south and stronger in the north of LPB, with decrease in the middle of the basin during ENM; little difference for LNM. ENC shows strong increase of extreme events in southern Brazil and LPB, while LNC tends to show opposite anomalies. In the period of study (1960-2008) there were more canonical events than Modoki events, and in the case of LN this difference is even greater. There are several regions in LPB with opposite impacts of Canonical and Modoki episodes.

September-October-November

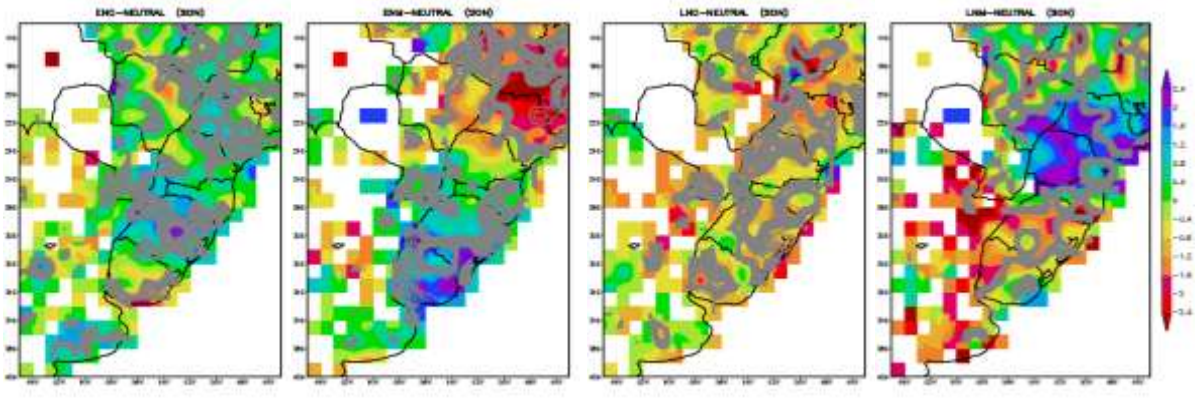

Canonical EN Modoki EN Canonical LN Modoki LN

March-April-May

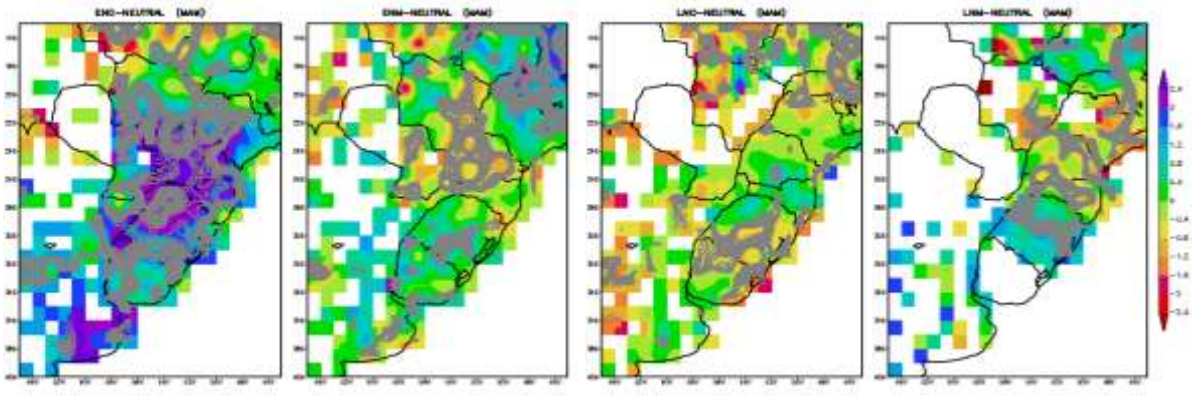

Canonical EN Modoki EN Canonical LN Modoki LN

Figure 2. Differences between observed numbers of extreme events in ENSO years and neutral years, for SON (upper panels) and MAM (lower panels), for different types of El Niño and La Niña episodes. Colors indicate the difference and the dark grey lines limit the areas where the difference are significant over the 90% confidence level.

3.2 CMCC (Zamboni and Cherchi) with the collaboration of CONICET (Carril). A characterization of heat waves

We have investigated the occurrence of summertime (DJF) heat waves (HW) over LPB, with the final aim of identifying their association with the large-scale circulation. We first underline that a unique definition of heat wave does not currently exist (Huth 2007, J. Climate, 20, 3802-3821). In our study, a heat wave is characterized by a period of at least two days in which the daily maximum temperature (Tmax) is above the 90th percentile. The choice of the 90th percentile follows the IPCC guidelines, while the minimum persistence results from our investigation, as it is discussed in the following. The daily 90th

percentile is calculated using a 5-days centered distribution over the period 1961-2000 at each location, hence the threshold is day and space dependent. This methodology allows filtering the intraseasonal variability as well as the local climatology, so that different regions can be easily compared, while considering a sufficiently large sample (5 days times 39 years) to create the distribution. The data used for the investigation are daily maximum temperature covering LPB for the period 1961-2000 at (0.5x0.5) resolution, and have been compiled by Tencer et al. (2010, AGU, 91(26), Meet. Am. Suppl., Abstract GC31A-10), within the CLARIS-LPB collaboration. In most cases sustained temperatures are isolated 1 day events. Over most of LPB there are (on average) 3 event/year, while sub-regions differ for ±1 event/3years. 2 days events are ~30% of the number of isolated cases, thus they are as frequent as 1event/year. As for isolated events, there is a slight tendency for more events to occur over the southern portion of the domain. More persisting events are remarkably rare: there are 1 to 2 events lasting three days every 3 years, and up to 1 event every 3 years lasting 4 days on average. Consequently, it is clear that extreme temperatures in LPB are short persisting events.

Even with an on average small number of cases, it is interesting to evaluate their interannual variability, in fact a higher variability, and thus the presence of a high number of occurrences in certain years, might indicate the existence of forcing factors. Tightly to the project's goals, we point out that in order to seek for a relationship with the large-scale circulation and GCMs' capability in reproducing it, the additional requirement of a basin wide extension of the HWs is needed. In other words, it is not expected that the large-scale circulation has very small scale impacts, nor that current state of the art GCMs are likely to reproduce small scale dynamics. Our requirement on the persistence of HW follows from the above considerations. With this definition, there are on average 2 HWs/year rather uniformly distributed over LPB, which present a fairly uniform distribution in time, and specifically years during which more than 4 events have occurred are less than 1/8 of the total period (Figure 3). Only three years were characterized by a large number of HWs interesting a broad spatial area over LPB, they are DJF of 1967/68, 1971/72, 1988/89 (Figure 4). We conclude that a systematic analysis on the relationship among the large-scale circulation and HWs over LPB cannot be pursued due to the lack of a sufficient number of occurrences. As a note we indicate that SINTEXG is able to capture the statistical properties of the occurrence of HWs even though the number of cases is slightly smaller.

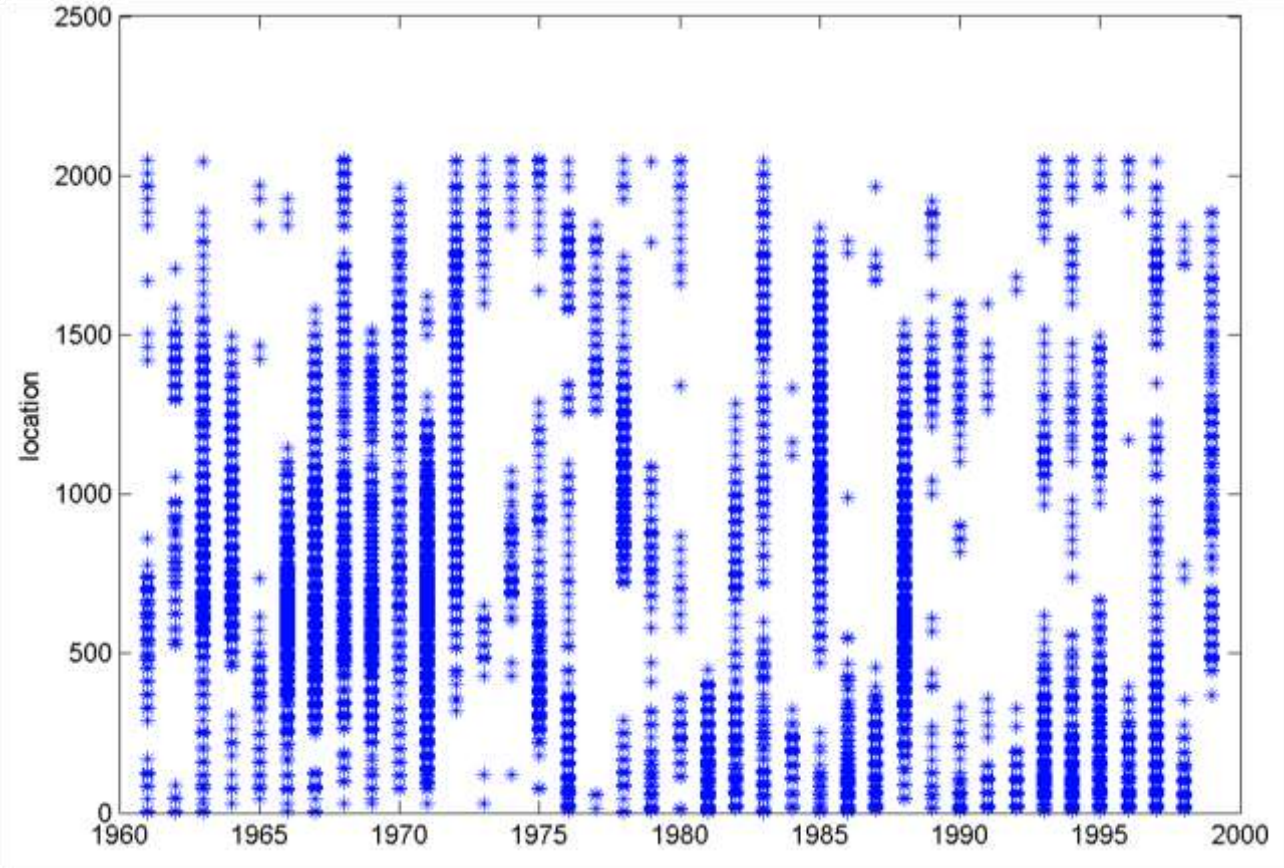

Figure 3. Space-time distribution of cases (*) in which more than 4 HWs have occurred at each location over LPB. Spatial points are ordered in columns from north to south, west to east. Few years present a fairly uniform band of cases at all points.

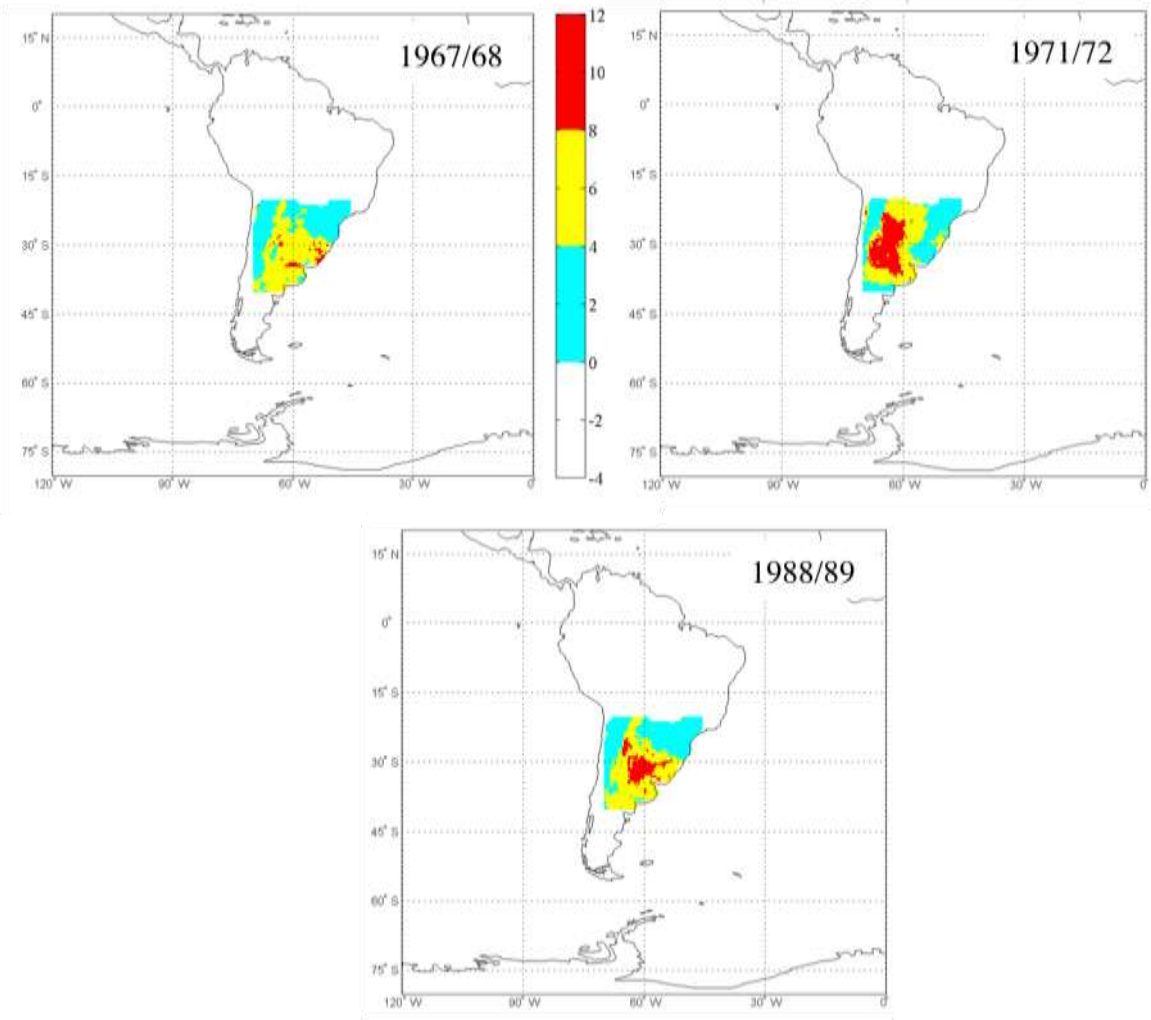

Figure 4. Total number of heat waves occurred in 1967/68, 1971/72 and 1988/89 DJF.

3.3 UBA (Rivera and Penalba). On the relationship between meteorological and hydrological droughts

Drought is a recurrent component of climate in La Plata Basin (LPB) and has extreme impacts on the hydrology of the region. The work performed during the last 6 months analyzes the relationship between meteorological droughts and hydrological droughts in the middle part of the Uruguay River. The Standardized Precipitation Index (SPI), which is the most widely used drought index, was used to characterize meteorological droughts at different time scales. In order to define the streamflow drought events in the region, we used the Q70 threshold, the flow which is equaled or exceeded for 70% of the time. The deficit volume (Q-Q70 monthly averages) was compared with the SPI considering two approaches: for the whole time series, considering all the months as a continuum, and seasonally, considering the Southern Hemisphere seasons. For comparison we used the Pearson correlation coefficient. In general, different studies indicate that there is a considerable time lag between departures of precipitation and the point at which these deficiencies become evident in surface components of the hydrologic system. Our findings prove that the surface runoff respond to short SPI time scales (2-4

months). The maximum correlation is found on the time scale of 3 months (SPI3; Figure 8). The seasonal comparison shows that the highest correlations were obtained in summer, which is the low flow season.

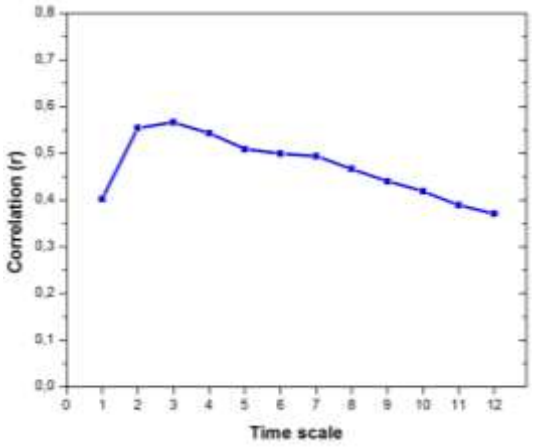

Figure 8. Correlation between Q-Q70 monthly averages and the SPI at different time scales.

We also made a comparison of the two time series for identified historical drought episodes. In the case of the extreme drought event, both the SPI3 and Q-Q70 shows similar behaviors (Figure 9), demonstrating their viability for studying time scales of various droughts and their interdependences. These results could be useful for forecasting and monitoring hydrological drought severity and in developing a drought preparedness plan in the region.

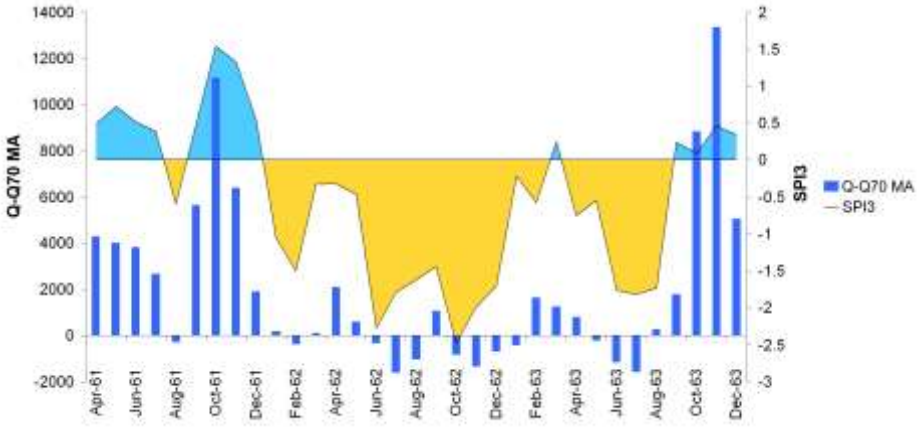

Figure 9. Graphical comparison of SPI3 and the deficit volume (Q-Q70 monthly averages) during the 1962/1963 extreme drought episode in Paso de los Libres station.

Moreover, by means of the SPI12, the year of the most extreme drought was determined for every pluviometric station analyzed, which are distributed along most of LPB. This was obtained by determining the minimum absolute value of the index over the total measurement period. Many of the stations with records starting in the 1920s and 1930s, which are located in the Central region of Argentina, had their most extreme drought during the 1930s. This could indicate that LPB experienced its worst drought during this period. In turn, for a large number of stations located in the eastern portion of the domain, which start their records between 1950 and 1970, it was determined the occurrence of its extreme drought during the 2000s (Figure 10).

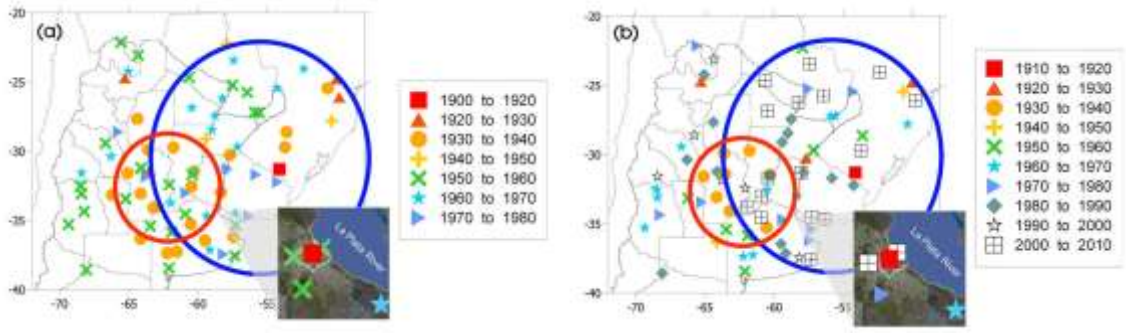

Figure 10. (a) Decade of the start of precipitation measurements. (b) Decade of most severe drought according to the SPI12 values.

3.4 UBA (Robledo, Penalba and Bettolli). Teleconnections between tropical-extratropical oceans and the daily intensity of extreme rainfall over Argentina

The main goal of this work is to identify the different ENSO regions of the oceans related with the extreme rainfall in Argentina, the tropical and subtropical Atlantic Ocean and the Indonesian Sea, in addition to areas of the Indian Ocean that influence Argentina's extreme rainfall. We have explored the covariability between sea surface temperature (SST) for all the oceans from 17.5º N to 90º S and the daily intensity of extreme rainfall in Argentina. This analysis was performed using a Singular Values Decomposition for three austral seasons (spring, summer and autumn). The analysis was performed in the period 1962 to 2005 using two data sets: monthly SST from the Kaplan SST V2 from the NCEP/NCAR and high quality daily rainfall for 35 surface stations from the National Weather Service of Argentina distributed throughout the country. The monthly mean of daily intensity of extreme rainfall index (DIER) is the quotient between the monthly accumulated extreme rainfall (AE) and the number of days with extreme precipitation events per month (PE). We consider extreme daily precipitation when rainfall is greater than the mean 75th daily percentile for the period 1961 to 2000. Equation 1 represents the DIER index and was performed for each of the 35 meteorological stations.

$$DIER_{i,j} = \frac{AE_{i,j}}{PE_{i,j}}$$

Equation 1. The daily intensity of the extreme rainfall index (DIERi,j). Where i represents months (1 to 12) and j represents the years (from 1962 to 2005).

The wavelet transform was applied to the SVD time series of the SST to analyze the dominant cycles and their period of occurrence. The five leading SVD modes of the coupled SST and DIER variations account for around 70 percent for summer and autumn and 80 percent for spring of the total square covariance (TSC). The large percentage of the covariance explained by the first SVD mode, for all seasons, suggests a fair degree of predictability between the DIER and SST. Spring registers the highest SCF –45 percent, whereas summer and autumn register 34 percent. These SST patterns have 4-year temporal cycles like the ENSO phenomena with an enhanced DIER in central and eastern Argentina. In the second SVD mode, spring has the highest SCF, 17 percent, whereas summer and autumn register 11 percent. For autumn and summer the tropical and subtropical Atlantic presents covariability with the DIER in central Argentina. Spring presents covariability in the Atlantic Ocean as well as in the Indonesian Sea. This mode shows a significant decadal variability with two sub-periods: 8 years and 12 years. In the third SVD mode of spring and summer the SCF are 10 percent and 6 percent, respectively; the Indian Ocean presents covariability with the DIER in the north and the eastern portion of Argentina, respectively. This mode shows a significant period of variability, around 14 years. In autumn the third mode presents a significant correlation of the tropical Atlantic Ocean and extreme rainfall in the center and eastern Argentina, with significant period of 14years. The SST regions identified in this study are another step in the continuing process of establishing the causes of low-frequency variability in the southern hemisphere.

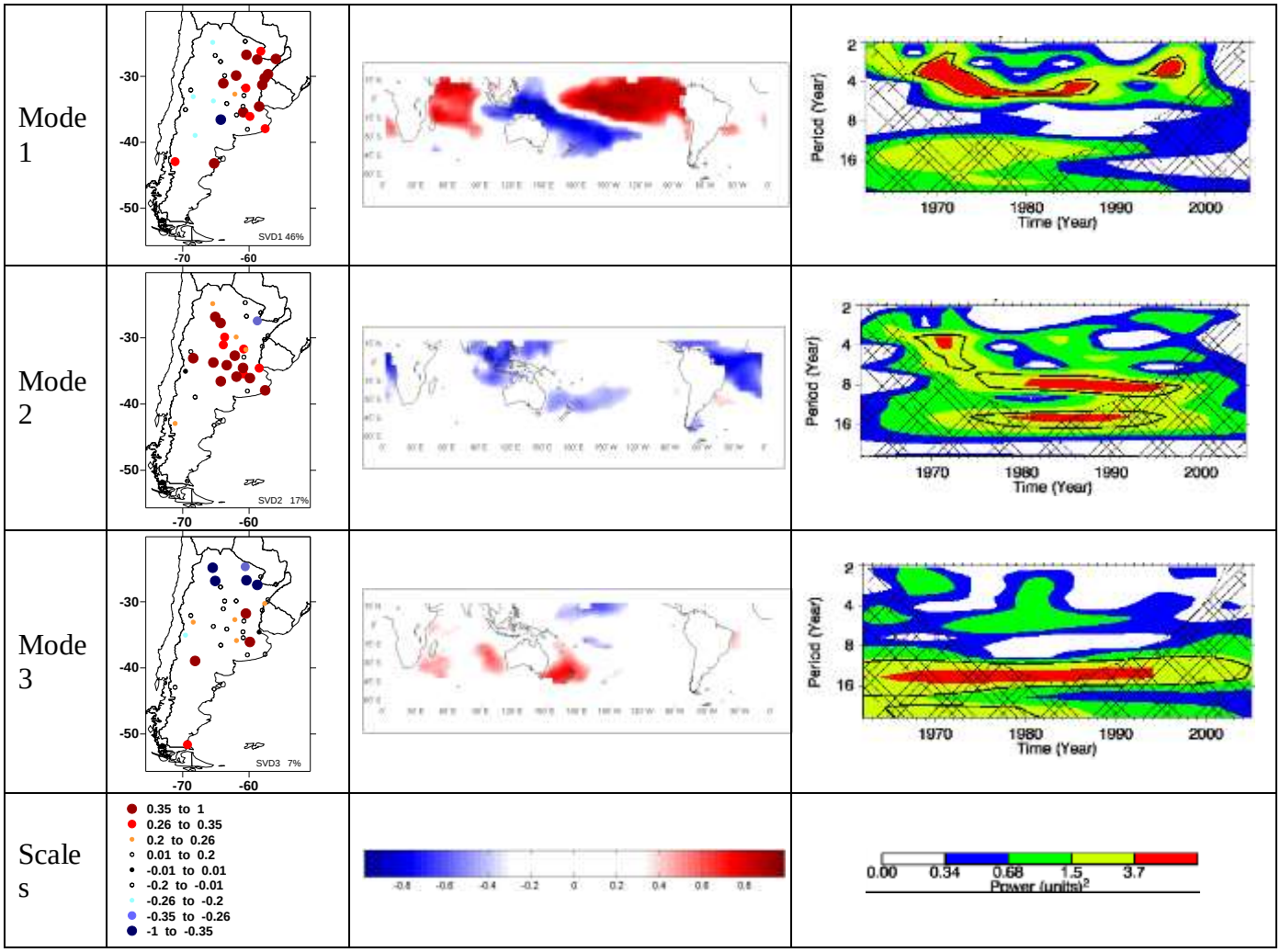

Figure 11 Spring Homogeneous Correlation maps for each mode. Grid point correlation between the time series of expansion coefficients of SST (a) and DIER (b) and anomaly patterns of each data set. Wavelet analysis of the SST time series of expansion coefficient (c).

3.5 UBA (Betolli and Penalba). Daily Sea Level Pressure Patterns in the GCMs

During this period our work was focused on clustering daily atmospheric structures (WTs) considering different variables, levels and periods/seasons. Daily rainfalls within the Argentine Humid Pampas are also investigated in connection to the weather type categories. Daily mean sea level pressure (SLP) fields corresponding to the NCEP Reanalysis 2 data provided by the NCEP-NCAR were used as representative of atmospheric circulation at low levels. The period of study was 1979-1999. The analyzed seasons correspond to summer (December-January- February) and winter (June-July-August). Daily rainfall series located in the central Pampas region were also used. Cluster analysis was performed coupled with Principal Component Analysis (PCA) to determine the atmospheric circulation patterns.

The most important results are summarized below: Summer sea level pressure daily fields were stratified into 5 weather type categories (Figure 12). Dry days are significantly favored by structures which denote

an intensification of the semi-permanent subtropical Atlantic high, inducing stability at low levels (WT2). This atmospheric structure (WT2) is one of the most persistent together with the weather type that resembles the mean pattern for summer (WT5). On the other hand, local rainy days are significantly benefited by patterns with a cyclonic disturbance at the center of the continent (WT4). This pattern (WT4) could be associated to a frontal passage and it is the less frequent (9.9%) of the season. It is also one of the less persistent pattern with the 88% of the events in sequences from one to three-day lasting. The most probable transition is WT5 >> WT1 followed by WT2>>WT5.

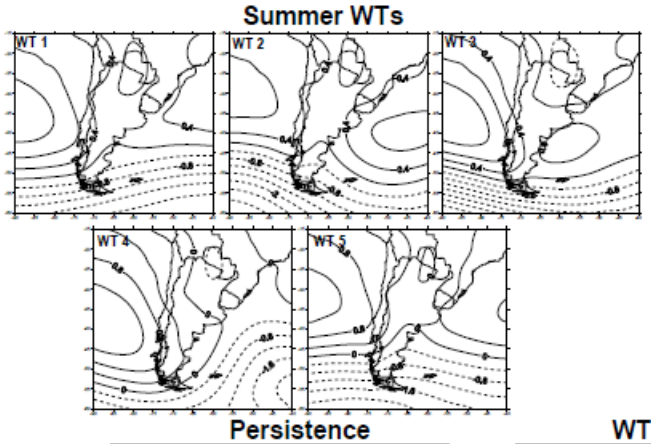

Frequency

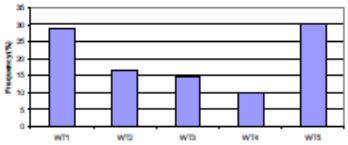

Persistence

D (days)	WT1	WT2	WT3	WT4	WT5
1	41,9	35,9	58,8	44,4	43,9
2	25,6	28,9	22,3	26,7	20,7
3	15,8	11,7	8,8	16,7	17,9
4	4,7	10,9	4,1	5,6	6,1
5	6,4	6,3	1,4	4,4	6,5
6	1,3	2,3	1,4		1,6
7	3,0	2,3	3,4	2,2	1,2
8	0,4	1,6			1,2
9					0,4
10	0,9				
11					0,4
12					

WTs and daily rainfall

	Dry Days	Local Rainy Days	Generalized Rainy Days
WT1	-1,2	-0,1	1,1
WT2	**3,3**	-1,3	**-2,8**
WT3	0,5	0,1	-0,4
WT4	**-2,3**	**2,3**	0,3
WT5	-0,3	-0,4	0,8

Z statistics of the comparison between the conditional probability of occurrence of a day with a certain rainfall condition in each circulation cluster and the climatological probability of that day. Bold: Significant values at 95%

Figure 12. Patterns, frequency and persistence of the synoptic weather types (WTs) and their relationship with daily rainfall in the central Pampas region for summer.

Winter sea level pressure daily fields were stratified into 7 weather type categories (Figure 13). Generalized Rainy Days are significantly benefited by structures with a high pressure system at the south of the continent, enhancing an anomalous flow from the east-southeast in the central region of Argentina and its corresponding moisture advection at low levels (WT3). WT4 also favours Generalized Rainy Days and could be related to a post-frontal anticyclone. WT3 is the less persistent pattern showing the 83% of the events in sequences of one- or two-day lasting. Dry days are significantly favoured by a high pressure system situated right inside the continent (WT5). The most persistent weather types for winter are also the most frequent ones (WT6 and WT7). The most probable transition is WT6 >> WT7 followed by WT1>>WT6.

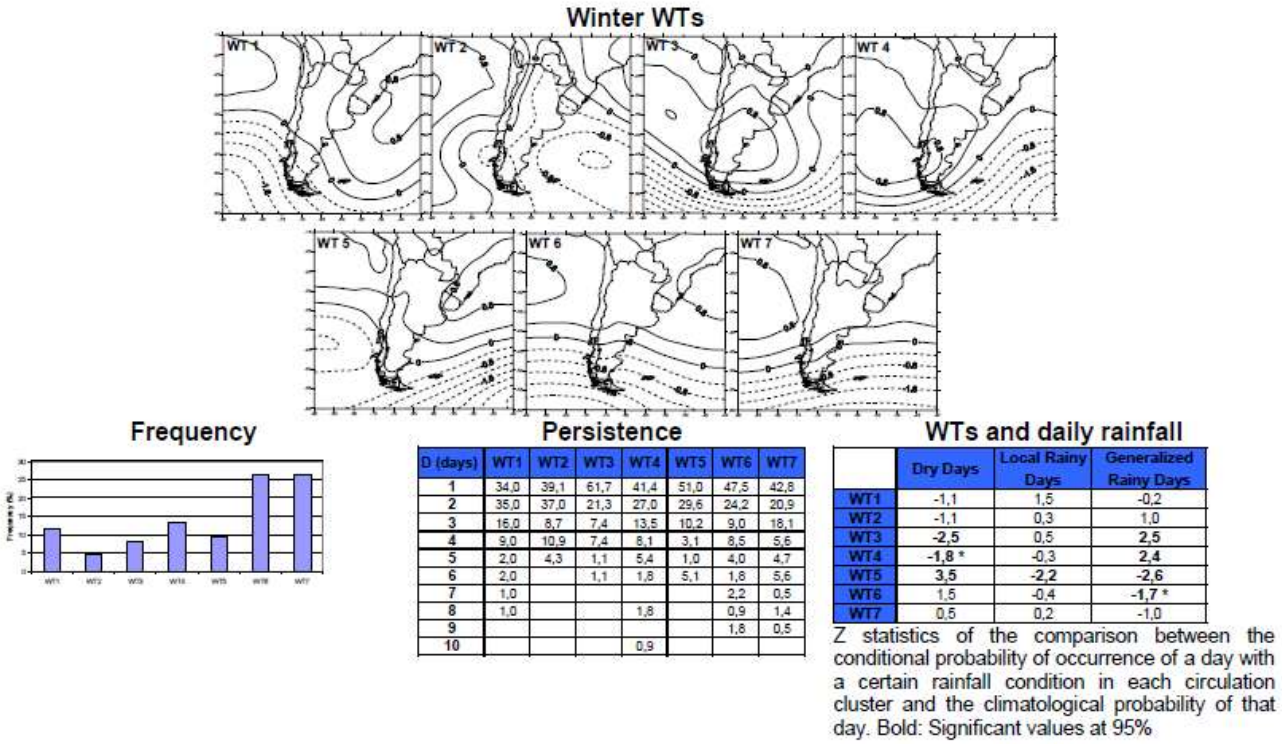

D (days)	WT1	WT2	WT3	WT4	WT5	WT6	WT7
1	34,0	39,1	61,7	41,4	51,0	47,5	42,8
2	35,0	37,0	21,3	27,0	29,6	24,2	20,9
3	16,0	8,7	7,4	13,5	10,2	9,0	18,1
4	9,0	10,9	7,4	8,1	3,1	8,5	5,6
5	2,0	4,3	1,1	5,4	1,0	4,0	4,7
6	2,0		1,1	1,8	5,1	1,8	5,6
7	1,0					2,2	0,5
8	1,0			1,8		0,9	1,4
9						1,8	0,5
10				0,9			

	Dry Days	Local Rainy Days	Generalized Rainy Days
WT1	-1,1	1,5	-0,2
WT2	-1,1	0,3	1,0
WT3	**-2,5**	0,5	**2,5**
WT4	**-1,8 ***	-0,3	**2,4**
WT5	**3,5**	**-2,2**	**-2,6**
WT6	1,5	-0,4	**-1,7 ***
WT7	0,5	0,2	-1,0

Z statistics of the comparison between the conditional probability of occurrence of a day with a certain rainfall condition in each circulation cluster and the climatological probability of that day. Bold: Significant values at 95%

Figure 13. Patterns, frequency and persistence of the synoptic weather types (WTs) and their relationship with daily rainfall in the central Pampas region for winter.

Our current work focuses in analyzing the GCMs ability to reproduce the basic characteristics of daily circulation at low levels and their relationship with daily precipitation. In order to achieve these objective daily outputs of 12 GCMs from the climate of the 20th century (20C3M) were downloaded in the period 1979 -1999 and the database was constructed. Because of the different resolutions of the models, it was necessary to re-grid SLP model outputs to the NCEP/NCAR reanalysis grid in order to facilitate comparisons.

3.6 CPTEC/INPE (Cavalcanti). Quantifying precipitation extremes

The numbers of extreme, severe and moderate precipitation cases, based on Standardized Precipitation Index (SPI) during the 1979-2001 period in the northern (NLPB) and southern (SLPB) are shown in Table 1 (GPCP), Table 2 (CPTEC) and Table 3 (HADCM3).

The main results are:

- Frequency of monthly wet extremes is higher than frequency of dry extremes (NLPB and SLPB) in observed (GPCP) and model results (CPTEC and HADCM3)
- Frequencies of wet cases are higher in the southern sector than in the northern sector in GPCP and the two models
- Frequency of wet extremes in CPTEC results is similar to GPCP in the northern sector, but it is higher in the southern sector. HADCM3 presents more wet cases than observed in both sectors

- Frequency of dry extremes is higher in CPTEC than in GPCP in the northern sector but lower in the southern sector. Less dry cases are identified in HADCM3 than in GPCP in both sectors
- LPBN: Higher freq. wet extremes in MAM : GPCP and CPTEC
- LPBS: Higher freq. wet extremes in MAM (GPCP) and DJF (CPTEC)
- Dry cases: no preference for any season (GPCP and CPTEC, N , S LPB)

	EW	SW	SW	ED	SD	MD
NLPB	6	15	25	3	12	24
SLPB	8	13	20	4	12	31

Table 1. Number of extreme, severe and moderate precipitation cases (GPCP).

	EW	SW	SW	ED	SD	MD
NLPB	6	12	26	5	13	23
SLPB	11	10	20	1	8	38

Table 2. Number of extreme, severe and moderate precipitation cases (CPTEC).

	EW	SW	SW	ED	SD	MD
NLPB	9	15	21	1	12	29
SLPB	12	8	22	2	7	30

Table 3. Number of extreme, severe and moderate precipitation cases (HADCM3).

3.6 CONICET (Carril, Menéndez and Sorensson). Assessment of extreme precipitation simulated by four regional models.

Simulations performed with regional models from the previous CLARIS FP6 project are being analyzed with emphasis in the study of temperature and precipitation daily extreme events. Four different models (LMDZ, PROMES, RCA3 and REMO) driven by reanalysis data (ERA40) were run at horizontal resolution of about 50 km. A multiyear simulation of the period 1991–2000 was performed with each model.

As an example of diagnostics being developed, Figure 14 shows Taylor diagrams for maximum (percentile 75, upper panel) and minimum (percentile 25, bottom panel) temperatures in summer (DJF) and winter (JJA) respectively. These diagrams are used to quantify and visualize the overall correspondence between CLARIS FP6 simulations (L: LMDZ, P: PROMES, Rc: RCA3, Re: REMO, E: ensemble mean) and the observational climatology (Tencer et al. 2010, a new temperature gridded daily data especially developed for this workpackage). Each model performance relative to the reference climatology is visualized by a point on the plot. Each point gives information on three basic statistics: correlation coefficient between modeled and observed data, standard deviation of simulated data, and

RMS difference between simulations and the reference data. Note that the spread between models is larger for the simulation of the maximum temperatures "extremes".

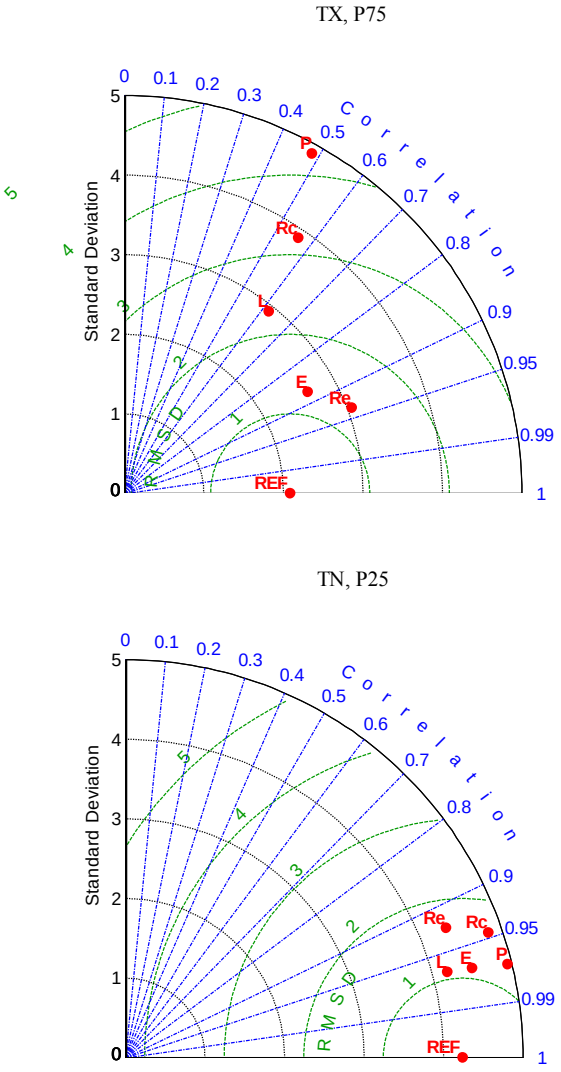

Figure 14. Taylor diagrams for percentile 75 of maximum and percentile 25 of minimum temperature (TX and TN) for DJF and JJA respectively. These diagrams are used to quantify and visualize the overall correspondence between CLARIS FP6 simulations (L: LMDZ, P: PROMES, Rc: RCA3, Re: REMO, E: ensemble mean) and observational climatologies (REF: CRU for precipitation and Tencer et al 2010 for temperature). Each model performance relative to the reference climatology is visualized by a point on the plot. Each point gives information on three basic statistics: correlation coefficient between modeled and observed data, standard deviation of simulated data, and RMS difference between simulations and the reference data.

3.7 UFP (Alice M. Grimm, Renata G. Tedeschi, Rafaela A. Flach and Aline B. G. Ingberman). The impact of canonical ENSO on extreme precipitation

Grimm and Tedeschi (2009) carried out the assessment of ENSO influence on the frequency and intensity of extreme precipitation events in South America, for each month of the ENSO cycle, based on a large set of daily station rainfall data, and compared it with the influence of ENSO on the monthly total rainfall. Significant ENSO signals in the frequency of extreme events are found over extensive regions of South America during different periods of the ENSO cycle. Although ENSO related changes in intensity show less significance and spatial coherence, they are robust in several regions, especially in the La Plata Basin.

The ENSO-related changes in the frequency of extreme rainfall events are generally coherent with changes in total monthly rainfall. However, significant changes in extremes are much more extensive than the corresponding changes in monthly rainfall, because the highest sensitivity to ENSO resides in the extreme range of daily precipitation in several regions of South America, especially the La Plata Basin. A preliminary analysis of the atmospheric anomalies associated with extreme precipitation events in the regions most affected during ENSO episodes was carried out. The stronger impact of ENSO on the extreme tail of the daily precipitation than on monthly rainfall totals in several regions of South America, especially the La Plata Basin, is related to the effect that ENSO has on the circulation anomalies associated with the extreme events in these regions, enhancing or hampering the main mechanisms leading to extreme events in these regions.

The more intense effect of ENSO on extreme events is relevant, since the most dramatic consequences of climate variability result from changes in extreme events. In view of this effect, an important issue is the assessment of the influence of global anthropogenic climate change on ENSO and its impacts, specifically its impact on extreme rainfall in South America. This assessment has been carried out in UFPR. First, by examining the influence of ENSO episodes on the frequency of extreme precipitation events in South America as simulated by the coupled models ECHAM5-OM and HadCM3 in the twentieth century climate (1960-2000), and comparing it with the observed influence. Second, by the analysis of projections of future climate, under emission scenario A2 (2060-2100), in order to evaluate the influence of climate change on the ENSO influence.

The EN and LN years in both, observations and model output, are determined from the Niño 3 SST anomalies, and verified against the extreme phases of the ENSO mode of SST variability in the model. Although the ENSO episodes in the model do not coincide with the dates of the observed episodes in the present climate (1960-2000), the statistical characteristics are very similar, and the ENSO cycle is reasonably well simulated. The results for only three months of the ENSO cycle and for ECHAM5-OM are shown here. Table 4 gives a quantitative idea of the ENSO impact on the frequency of extreme events in the western part of Southern Brazil, in the La Plata Basin (LPB).

Month	***El Niño (11 years)***	***La Niña (9 years)***	***Neutral (27years)***
November *April*	*6.2* *5.6*	*1.2*	*2.5* *2.8*

Table 4. Average number of extreme rainfall events in the western part of southern Brazil.

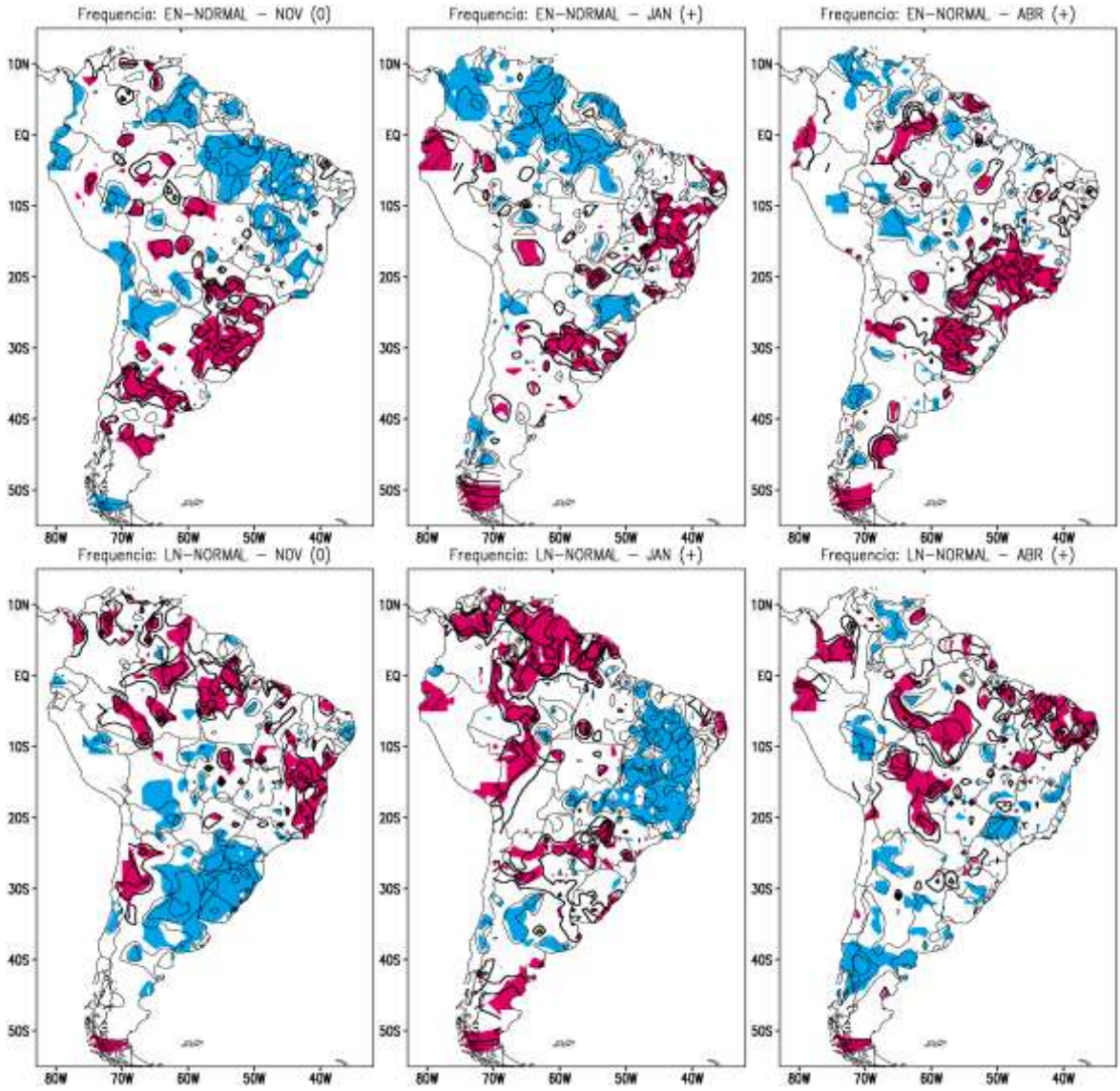

Figure 15. (Upper panels) Differences between observed numbers of extreme events in El Niño years and neutral years, and (lower panels) between numbers of extreme events in La Niña years and neutral years, for (Left) November (0), (Middle) January (+) and (Right) April (+). Contour interval is 1 event. Positive (negative) differences significant over the 90% confidence level are represented by red (blue) shade (adapted from Grimm and Tedeschi 2009).

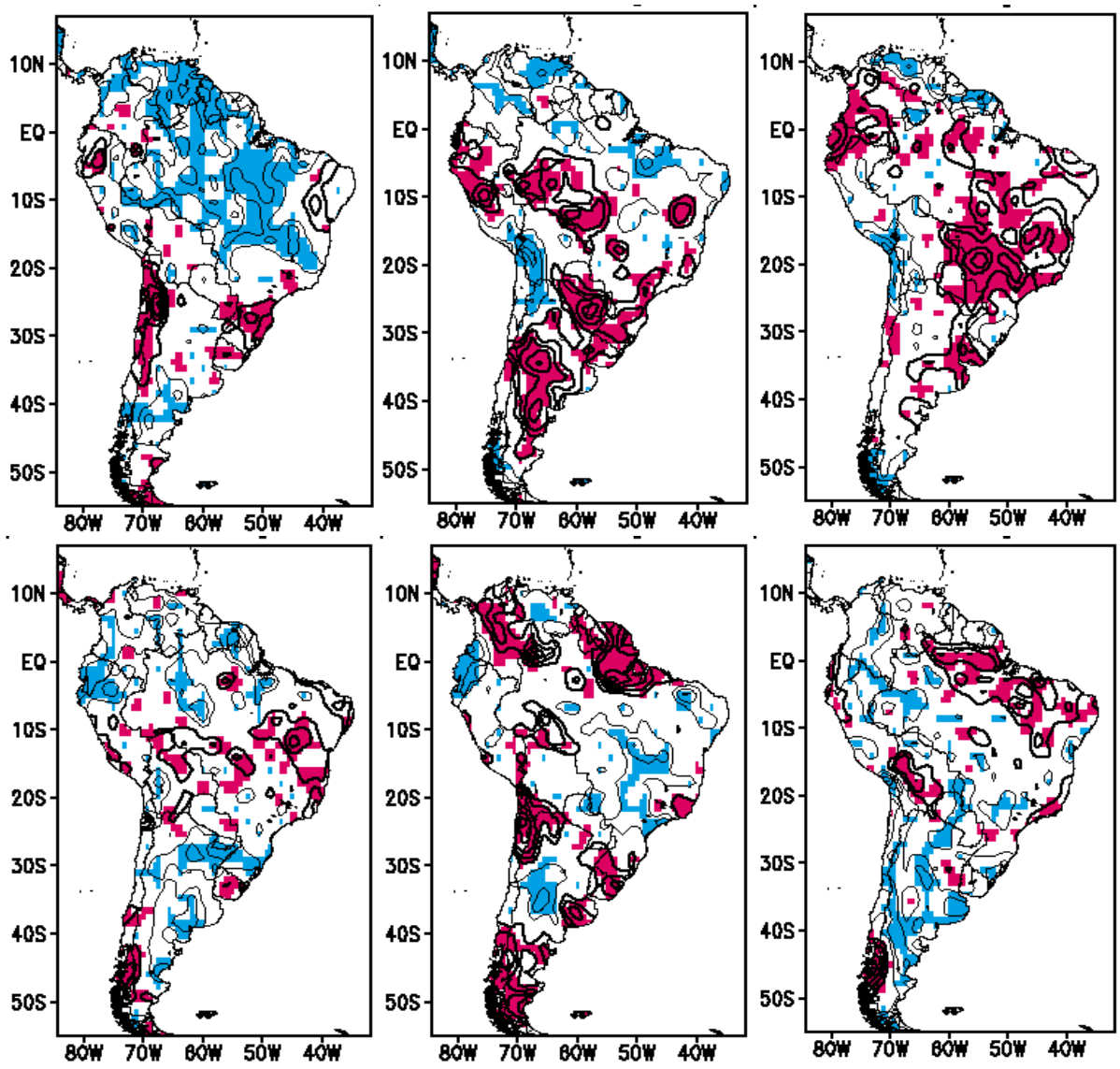

Figure 16. Same as Figure 15, but for simulation of present climate by ECHAM5-OM (1960-2000).

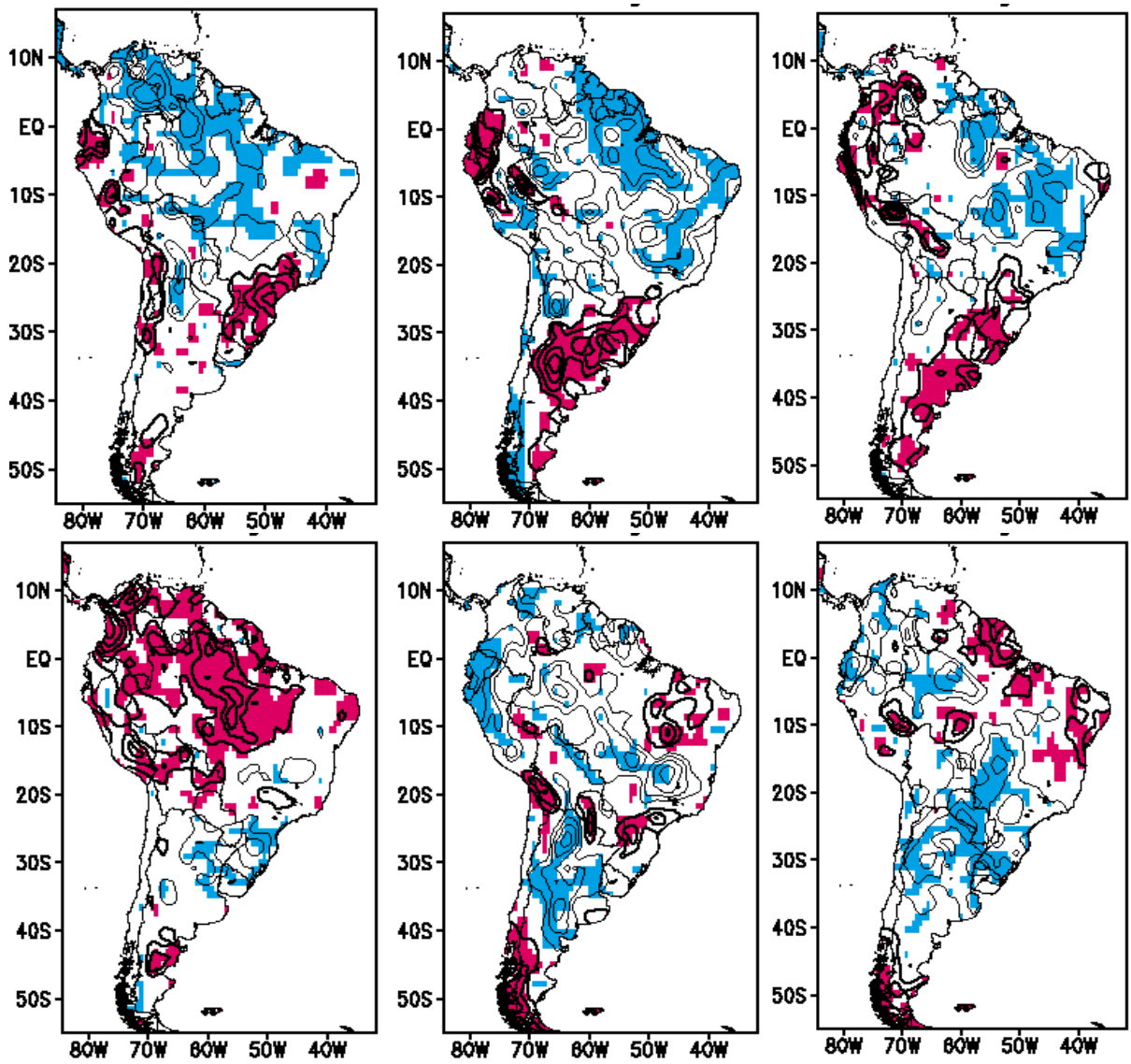

Figure 17. Same as Figure 15, but for projection of future climate by ECHAM5-OM (A2, 2060-2100).

Figure 15 shows the observed influence of ENSO on the frequency of extreme events, for three months, in the period (1960-2000) (Grimm and Tedeschi 2009). Figure 16 shows the impact of ENSO as simulated by the model ECHAM5-OM. From Figures 15 and 16, it is possible to see that the ENSO impact on extreme events in November (0) is well represented by the model during El Niño episodes, with the exception of southernmost South America, although the impact is underestimated in the LPB. The impact is also underestimated during La Niña episodes. Yet in January (+) the model overestimates the impact in the LPB during El Niño episodes and does not reproduce well the impact during La Niña episodes. In April (+) the impact of El Niño is very well reproduced, during El Niño and La Niña episodes. It is interesting to see that the model tends to reproduce the reversal of impact in the northern part of the LPB from November (0) to January (+), as seen in the observed data (Grimm and Tedeschi 2009). Figure 3 shows the ENSO impact on the frequency of extreme events in the future climate under emission scenario A2 (2060-2100). Comparing Figures 16 and 17 we notice that ENSO impact on extreme events strengthens in November (0), both during El Niño and La Niña episodes, in LPB. The same tendency is not generally visible in LPB in January (+) or April (+), although in Southern Brazil the number of extreme events is enhanced in the future climate. Figure 18 shows the distributions of daily rainfall for November (0) of El Niño years in a region in Southern Brazil, which show clearly the enhancement of heavier rainfall and extreme events in the future scenario, while episodes of light rainfall are reduced. It is interesting to point out that the more extensive significant changes in extremes than changes in monthly rainfall, observed during ENSO events, are also visible in the model output, for the present and future climate.

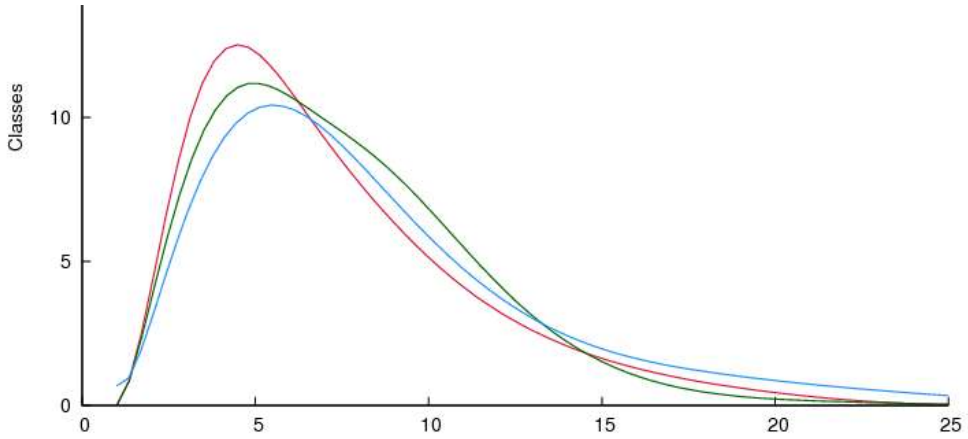

Figure 18. Distributions of daily rainfall of ECHAM5-OM for November (0) of El Niño years in a region in Southern Brazil, for (red line) present climate (1960-2000) and (blue line) future climate (A2, 2060-2100).

The following conclusions can be drawn from the results (not all shown):

- EN and LN episodes influence significantly the frequency of extreme precipitation events in several regions of South America during certain periods of the ENSO cycle. Most of the impact occurs during the rainy season.

- The impact of ENSO on extreme events is more significant and extensive than on monthly or seasonal precipitation totals. There is more sensitivity to ENSO in the extreme ranges of daily rainfall.
- The frequency of extreme events increases (decreases) when the large-scale perturbations associated with ENSO favor (hamper) the circulation anomalies associated with extreme events in the affected regions. This happens frequently during ENSO events.
- ECHAM5-OM reproduces reasonably the impact of ENSO on extreme events. The future scenario A2 shows enhancement of extreme events in the Basin with respect to the present impact of El Niño.
- The histograms of daily rainfall in November in La Plata Basin show reduction (increase) of frequency of light (heavy) rainfall from the present to future climate, especially during both El Niño and La Niña years, which reduces the overall ENSO impact on the region.

3.8 SMHI, Rossby Centre (Nikulin and Samuelsson). Evaluation and future projections of the simulated precipitation extremes over South America

Possible climate changes in extreme events need new adaption and risk management strategies that take into account how the statistics of extreme events may change in the future. On regional scale such information can be derived from simulations performed by regional climate models (RCMs). First of all it is important to know how RCMs reproduce the main aspects of the observed extreme events. We evaluate three RCMs (SMHI-RCA35, CIMA-MM5 and UCLM-PROMES) in their ability to simulate precipitation extremes over South America. All three simulations are driven by the ERA-INTERIM reanalysis and cover the 1990-2008 period. Observations with high spatial and temporal resolution are needed for evaluation of the simulated precipitation extremes on regional scale and here we use the Tropical Rainfall Measurement Mission (TRMM, version 3B42, 1998-2008) data set. The precipitation extremes are expressed in terms of the 20-year return values and because the period is rather short we apply the Generalized Pareto distribution (GPD) that is fitted to the 30 most intense daily accumulated precipitation (P_{max}) sampled at each grid point. In addition the 99th percentile is calculated for the same period 1998-2008.

The projection of possible future changes in precipitation extremes is based on an ensemble of three simulations performed by the SMHI-RCA35 (1961-2100) that is driven by the ECHAM5 (A1B emission scenario) and these 3 members are different only in initial conditions. Such en ensemble allows us to estimate uncertainties related to natural variably. The block maxima method and the Generalized Extreme Value (GEV) distribution are applied for these simulations to estimate the 20-year return levels. Analysis is performed for all four seasons and as example only the December-February (DJF) season is presented.

Figure 19 displays the 20-yr return value of P_{max} ($P_{max,20}$) in DJF estimated from the TRMM and biases of RCMs and their ensemble mean. The $P_{max,20}$ estimates from the TRMM may reach up to 200-250 mm/day, over some parts of the La Plata Basin (LPB) for example, but in many regions (in white) the $P_{max,20}$ cannot be calculated because of small amount of precipitation. Spatial patterns of biases for the simulations show a complex, noisy structure but some common features that can be identified are an overestimation over the Amazonia and Andes and a underestimation over northern part of South America and the LPB. Using the 99th percentile to express extreme precipitation helps to reduce noise in the bias patterns (Figure 20) where the biases are more clearly seen. As expected the estimated 99th percentile from the TRMM is less intense (up to 100 mm/day) than the $P_{max,20}$ since represents the threshold for the

10 strongest events occurring in the 1998-2008 period. The ensemble mean bias on average smaller than the individual biases and the ERA-INTERIM bias especially for the 99th percentile.

The projected climate changes in the $P_{max,20}$ for 3 simulations (DJF) and for the 3 subsequent 30-year periods is shown in Figure 21. Despite of noise related to natural variability all simulations and especially the ensemble mean show similar tendencies to less intense extreme precipitation over eastern Pacific and more intense one over the LPB and northern part of South America. To illustrate the role of natural variability in the projected changes we perform the 30-year moving GEV fit over southern LPB region (65°W-55°W, 38°S-32°S, only land) that results in time series showing time evolution of the simulated climate changes over this region (Figure 22). As we see from Figure 22 the projected changes in precipitation extreme can be very different among the simulations driven by the same ECHAM5 model but different only in initial conditions. For example, around 2020, one simulation (r2) shows a small decrease - 2 mm/day while other one (r3) shows a large increase - 20 mm/day. Differences about the same magnitude between two simulations are also evident for the 2070-2080 period. Such large natural variability in the simulated precipitation extremes results in very noisy patterns shown in Figure 21 since the $P_{max,20}$ is an estimation for only one specific 30-year period. The ensemble average in Figure 22 smoothes decadal variability and shows an increase in intense precipitation over southern LPB with large multi-decadal variability after 2050 that most likely is originated in the driving ECHAM5.

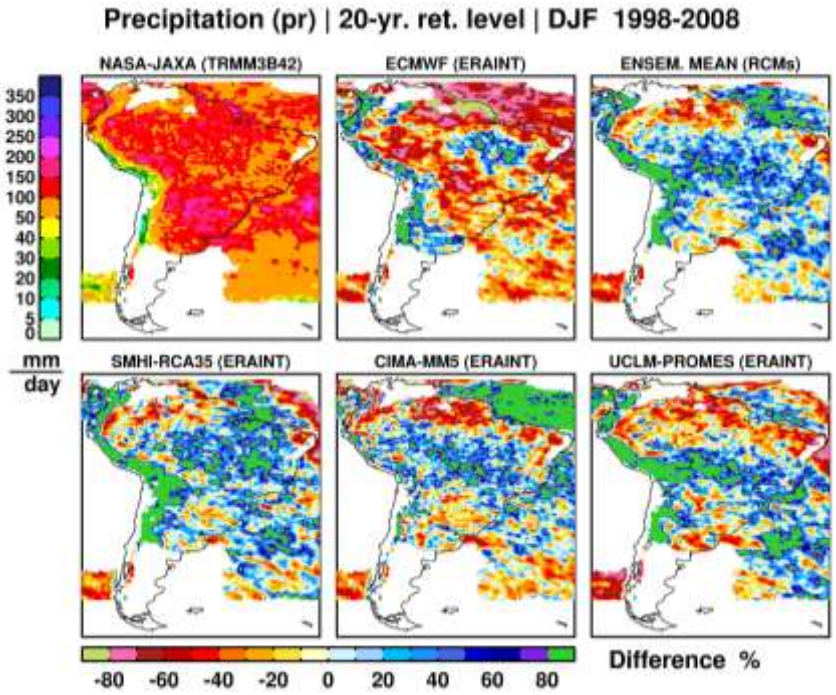

Figure 19: $P_{max,20}$ estimated from the TRMM data and biases of $P_{max,20}$ estimated from the ERA-INTERIM, three different RCMs driven by the ERA-INTERIM and their ensemble (DJF, 1998-2008).

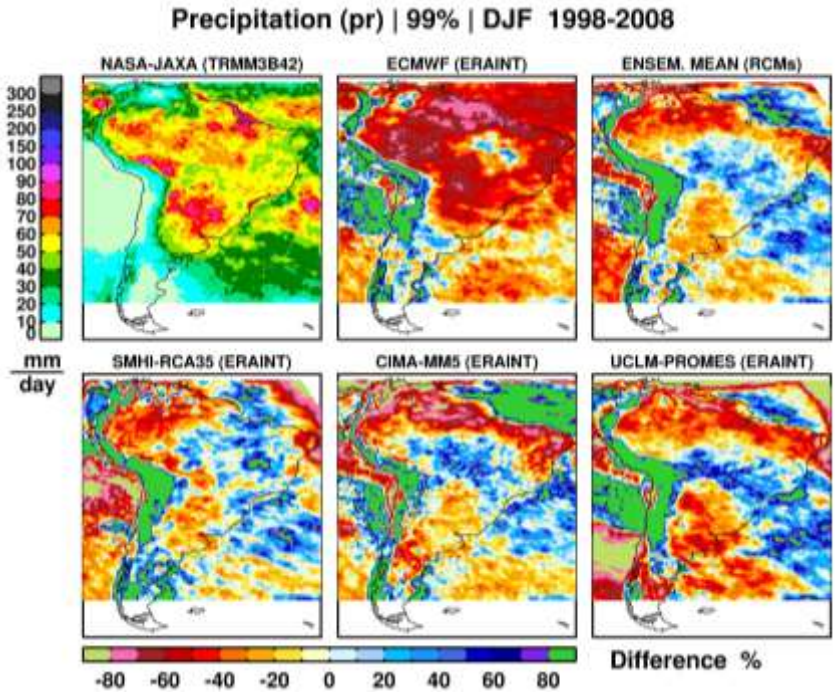

Figure 20: The same as Fig.19 but for the 99th percentile of daily accumulated precipitation.

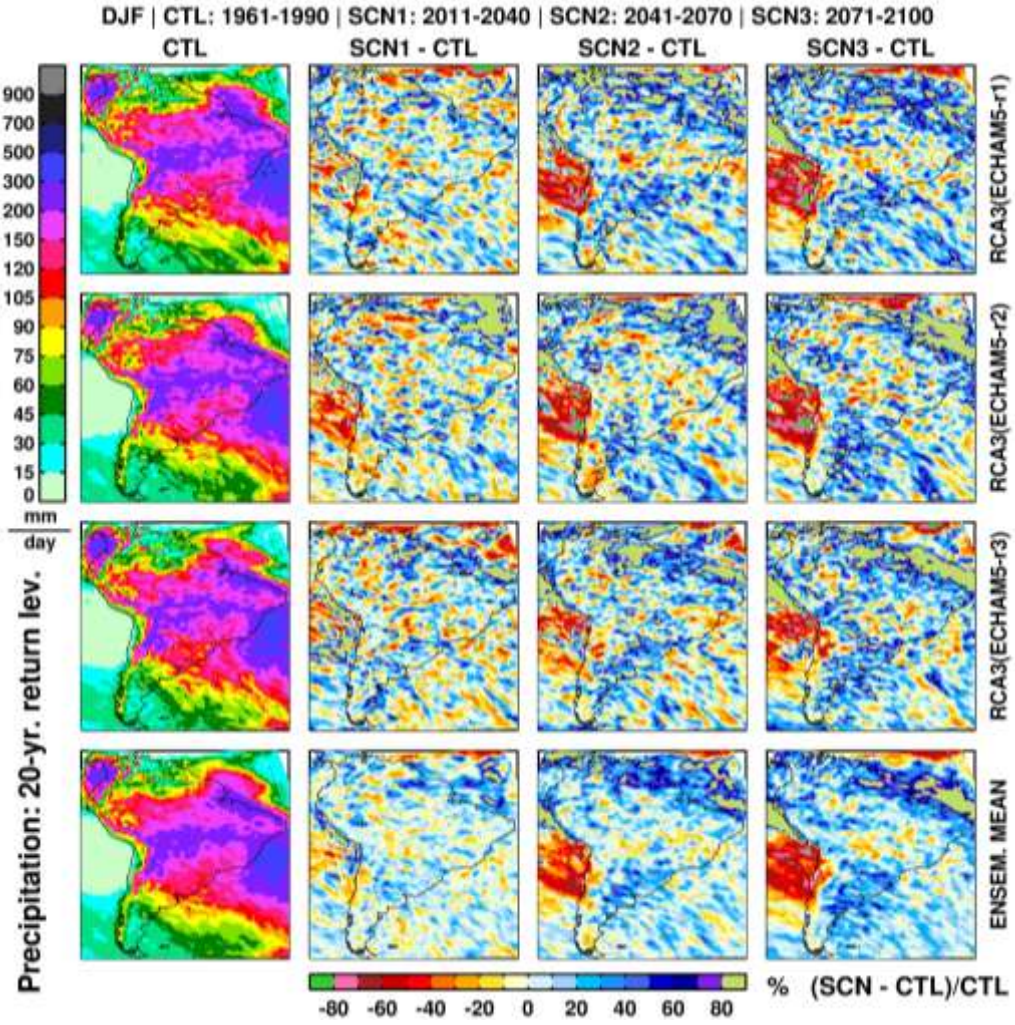

Figure 21: $P_{max,20}$ estimated from three SMHI-RCA35 simulations driven by the ECHAM5 (r1, r2, r3) and their ensemble mean for 1961-2100 (left column) and the respective changes in 2011-2040, 2041-2070 and 2071-2100 compared to 1961-1990 in the three rightmost columns.

Both evaluation and future projection of precipitation extremes presented in the study illustrate importance of the ensemble mean approach. The multi-model averaging provides more accurate representation of the observed precipitation extremes that most of the individual runs, though only three RCMs may be not enough. Anthropogenic signal in precipitation extremes may be masked by large natural variability if we choose only one or several time slices like in Figure 21. One way to identify the signal in more robust sense is to plot time evolution of the projected climate changes over regions applying a moving window approach (Figure 22).

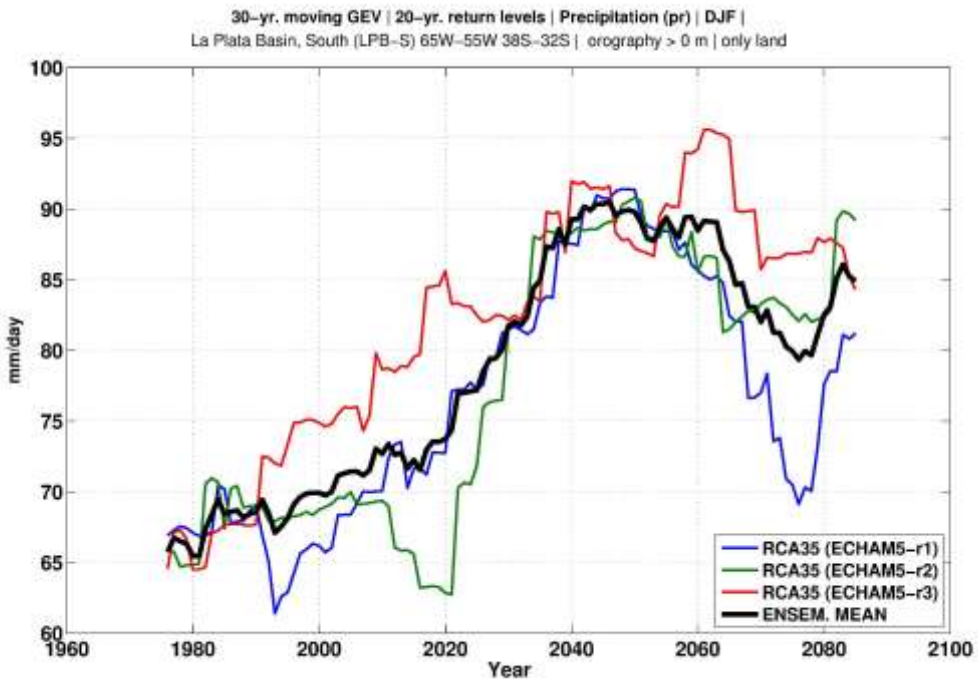

Figure 22: $P_{max,20}$ estimated by the 30-year moving window from three SMHI-RCA35 simulations driven by the ECHAM5 (r1, r2, r3) and their ensemble mean over southern La Plata Basin (65°W-55°W, 38°S-32°S, only land).

Other initiatives that complement the specific tasks of WP6

USP (Ambrizzi and Rocha)
Can Indian Ocean SST anomalies influence South American rainfall?

In this study the impact of the Indian Ocean sea surface temperature (SST) variability onto South American circulation was examined. Previous studies have shown that the Indian Ocean Dipole (IOD) mode can affect climate over remote regions across the globe, including over South America. Here it is shown that such link exists not only with the IOD, but also with the Indian Ocean basin-wide warming (IOBW). The IOBW, a response of El Niño events, tends to reinforce the South American anomalous circulation associated with the warm events in the Pacific, leading to increased rainfall in the La Plata basin and below-average precipitation over the northern regions of the continent. In addition, the IOBW is suggested to be an important factor modulating the persistence of dry conditions over northeast Brazil during austral autumn. Numerical simulations using a Global Circulation Model have also confirmed these results. The link between the IOBW and South American climate occurs via alterations of the Walker circulation pattern through the Atlantic Ocean and via a mid-latitude wave-train teleconnection.

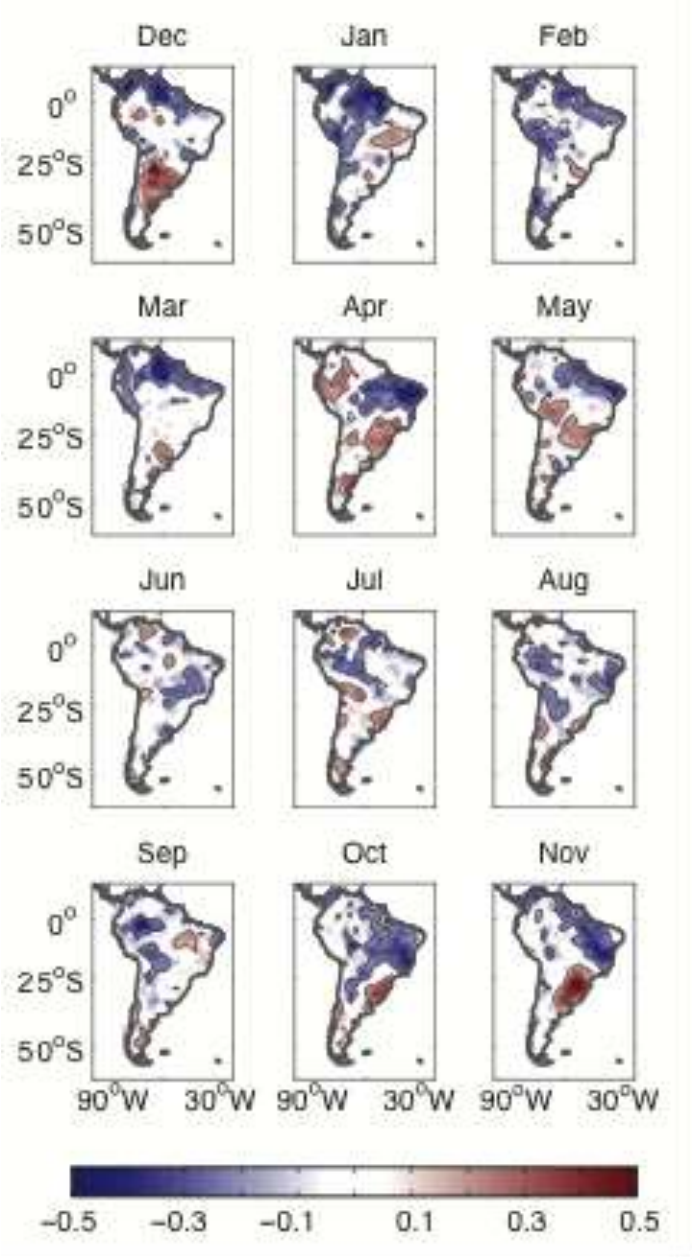

Figure 23: Monthly correlations between South American precipitation and the Indian Ocean basin-wide warming. The areas within the thin black line are significant at the 0.1 level.

The relation between the IOBW and precipitation over South America is accessed via correlation analysis (Figure 23). Monthly correlations reveal significant coefficients over the north and northeast regions of South America, as well as the La Plata basin, particularly strong from October to May at both regions.

In order to investigate the mechanisms associated with the IOBW onto South America, we assess how well this relationship is captured by the NCAR CAM3 model. Figure 24 shows the month-by-month correlations between the IOBW and the simulated South American rainfall from the Global Ocean experiment. It is notorious that the model tends to overestimate the correlations between the Indian Ocean and South America rainfall compared to observations. This is due to the fact that we use an

ensemble mean instead of a single simulation for the correlation analysis. The ensemble mean smoothes variations associated with internal variability while at the same time highlights the external signal related to the SST forcing.

Despite overestimating correlation maps, the NCAR CAM3 appears to represent quite well the seasonality of the relationship between the IOBW and rainfall, with correlations decreasing considerable during austral winter and enhancing from spring to autumn. In addition, the model seems to capture satisfactorily well the dipole structure seen in observations from October to May (compare Figures 23 and 24). A reduction in rainfall is simulated over north South America while an increase in precipitation occurs in the southeast, when the tropical Indian Ocean is anomalously warm.

Observations and experiments shown so far support the idea that the IOBW holds a statistical link with precipitation over the northeast South America. In the subtropics, the La Plata rainfall reveals significant correlations with the IOBW during October to May. This signal appears to be connected with the tropical Indian Ocean via a mid-latitude stationary Rossby wave-train pattern, as shown by anomalies of asymmetric streamfunction. In the reanalysis, the wave-train pattern is less defined over the Indian Ocean sector when compared to the simulations. This is due to the relative low magnitude of the IOBW compared to El Niño events and to the difficulty in separating the impact of these episodes. A cyclonic circulation is located over the South Atlantic inducing an offshore flow over the La Plata basin. This flow strengthens the low-level jet and consequently enhances the transport of moisture to the subtropics in the continent (Silva and Ambrizzi 2009). The result is an increase in rainfall over South American subtropics, a common characteristic from El Niño events.

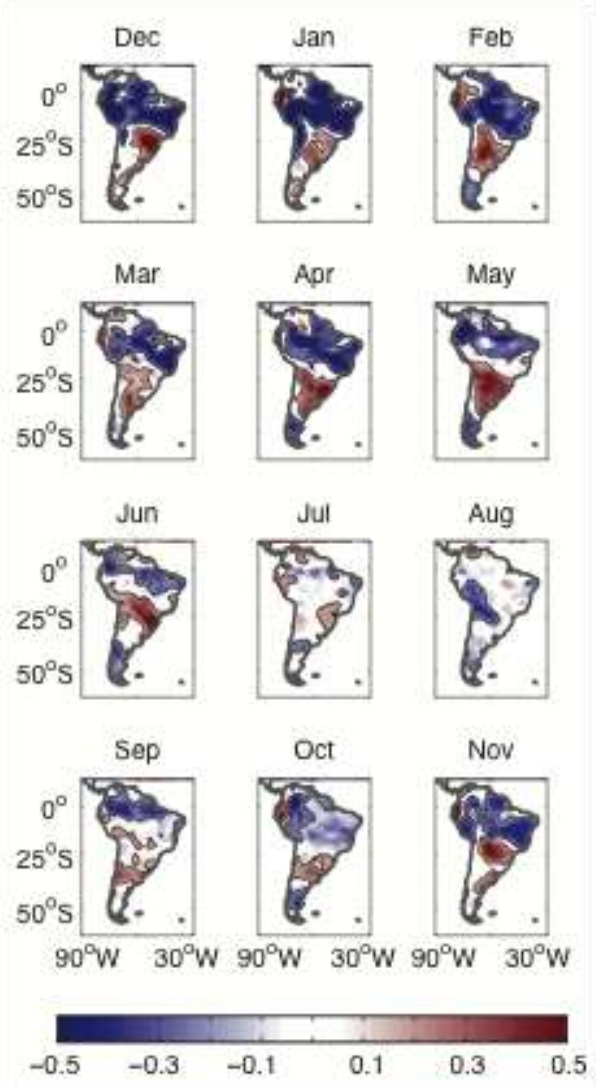

Figure 24: Month-by-month correlations between the IOBW and simulated South American rainfall from the Global Ocean experiment. Areas within the thin black line represent correlations significant at the 0.1 level.

USP (Ambrizzi and Rocha)

Certainties and uncertainties about reanalysis data and their usefulness on the study of extreme precipitation events over the La Plata basin

The main objective of this work is to evaluate bias on different reanalysis data as well as surface station data interpolated on a regular grid compared to observational data.

It will be analyzed the differences among the datasets during extreme precipitation events over the La Plata basin. The data used are from the NCEP reanalysis, ERA 40 from ECMWF, precipitation from CPC and surface station data available from the CLARIS-LPB project. Again, some simple statistical techniques such as sampling distributions, parameter estimation, linear regression and others were applied to the data.

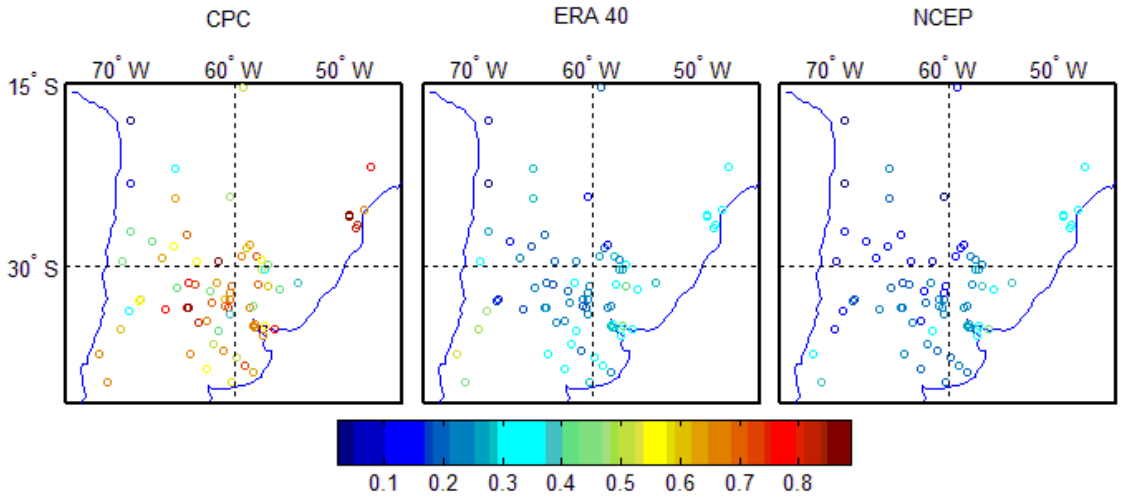

Figure 25: Simple correlation analysis between rainfall observational data and data from CPC, ERA40 and NCEP for the period 1979-2002.

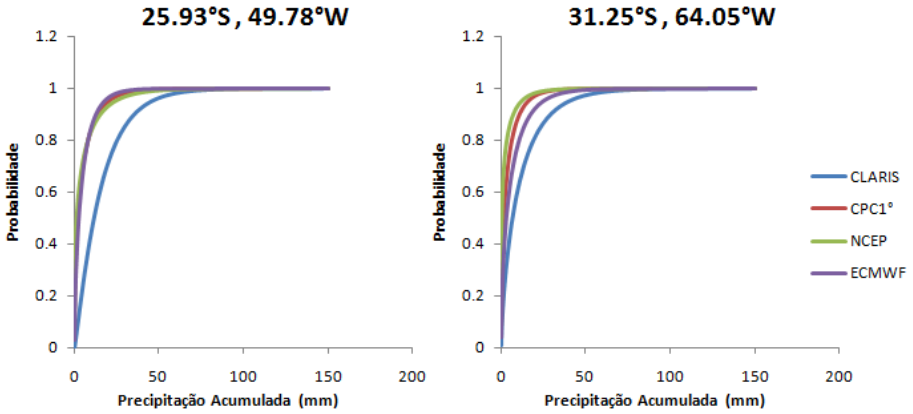

Figure 26: Cumulative Distribution Function (CDF) between the CPC, NCEP and ERA40 data and the precipitation from two CLARIS LPB meteorological stations.

From Figure 25 it is clear that the data the reanalysis (NCEP and ERA40) have lower correlation when compared to the CPC. On the other hand, Figure 26 indicates that all those data underestimate the precipitation compared to the CLARIS-LPB data. From the results above it is clear that studies of extreme precipitation event that use any reanalysis data or even station data interpolated in a regular grid will underestimate the amount of rainfall. Further analysis is currently in progress to evaluate how strong the bias is.

4. Next steps and conclusions

A summary of the discussions carried during the meeting is displayed bellow.
First, the next steps related with the ongoing work partner by partner are summarized. Then, the conclusions of wp6 meeting related with plans for coordinated works and suggested inter-work package feedbacks are presented.

4.1 Next steps by partners

CONICET
Extremes in regional and global models

Next steps are …

- A cross wp6/wp5 initiative: to collaborate with the validation of the novel ensemble Solman in collaboration with Carril et al.
- A cross wp6/wp4 initiative: to collaborate studying extremes in ENSO flavors Carril and coautors

CPTEC/INPE
Extreme monthly precipitation over two sectors of LPB -observations and simulations from CPTEC/COLA AGCM and HADCM3
Cavalcanti

Next steps are …

- The frequency analysis during INTERIN period from Regional models and station data
- The teleconnection analysis

Rossby Centre, SMHI
Evaluation and future climate projections of weather extremes over South America
Nikulin, Samuelsson

Next steps are…

- To check quality of the TRMM data in estimation of extreme precipitation
- To perform similar analysis for a larger ensemble: more RCMs (may be more driving GCMs)
- To include more regions in analysis
- To identify physical mechanism related to the projected changes in temperature and precipitation extremes

CMCC
A characterization of extremes over South America
Zamboni, Cherchi

Next steps are…

- The collaboration with CONICET in a cross wp4/wp6 initiative extremes in ENSO flavors (the database for the analysis will be integrated by CMCC)

UFP
Canonical and Modoki-ENSO and influences on LPB precipitation extremes
Tedeschi, Grimm (in collaboration with Cavalcanti/CPTEC)

Next steps are…

- To explore the characteristics of atmospheric fields during extreme events in some regions, for each category of years of ENSO;
- To analyze extreme events during ENSO years for some global models (GFDL, HadM3 and CPTEC), present climate;
- Idem, for climate change scenarios

UBA
Working on hydroclimate extremes….
Penalba et al

Next steps are…

- Analyze the relationship between atmospheric and oceanic conditions associated with the occurrence of droughts and extreme hydrological condition (water balance) in La Plata Basin.
- Study the effects of SST in the Pacific Ocean in the extreme daily rainfall in SESA. Compare this signal with the ENSO events and Modoki. Characterize the atmospheric conditions associated to these extreme conditions
- Investigate potential predictors of precipitation in selected regions in La Plata Basin.

4.2 Plan for coordinated works

In order to sucesfully reach D6.5, a series of coordinated initiatives was proposed

- Cross wp5/wp6 initiative: Solman in collaboration with Carril (CONICET) will lead a paper "on the validation of the regional climate models focusing on extremes".

- Cavalcanti (CPTEC) will lead an initiative on extremes (to be discussed).

- Nikulin (SMHI) will lead an initiative "on the analysis of extremes in time slides of the continuous RCMs integrations, present and future climate"

- Cross wp5/wp6 initiative: Marengo (CPTEC) will lead a paper about "droughts over Amazonia using the RCMs"

- Cross wp4/wp6 initiative: Carril (CONICET) will lead one of the following initiatives: "Extremes in different ENSO flavors" or "Extremes in LPB related with SST changes in the context of global warming"

4.3 Suggestions - Cross work package activities

4.3.1 A suggestion from WP3: homogeneous indices

It was suggested to produce indices (wp6/wp3/wp5/wp7 interphase)

- First idea is to estimate indices from homogeneous codes in different datasets. The suggestion was to use the fortran code from ETCCDI Climate Extreme Indices dataset.

- Another input is to start interacting with groups working on the "Atlas of Extremes for the Americas" (work on progress, VAMOS) → Cavalcanti (CPTEC) is participating on this activity. To promote the CLARIS – VAMOS groups interaction. Cavalcanti was proposed as the natural leader for this activity (to be further discussed).

4.3.2 Special request of WP8: A map of extremes

- On the one hand, WP6 is going to contribute by delivering the information requested by WP8 (WP6 will wait for WP8 inputs) to build a regional maps highlighting extremes as observed during the last decades

- On the second hand, useful information (e.g., tends of particular extremes in different locations, frequency and intensity, etc.) will be collected by Boulanger to build the map.